Research article

Synthesis of silver nanoparticles using *Eucommia ulmoides* extract and their potential biological function in cosmetics

Jinfeng Xi [a,b], Wenjie Kan [d], Yan Zhu [a,b], Shengwei Huang [e,*], Lifang Wu [a,b,c,**], Jun Wang [a,b,c,**]

[a] *The Center for Ion Beam Bioengineering and Green Agriculture, Hefei Institutes of Physical Science, Chinese Academy of Sciences, Hefei 230031, Anhui, China*
[b] *University of Science and Technology of China, Hefei 230026, Anhui, China*
[c] *Zhongke Taihe Experimental Station, Taihe 236626, Anhui, China*
[d] *Institutes of Physical Science and Information Technology, Anhui University, Hefei 230601, China*
[e] *Institute of Biomedical and Health Science, School of Life and Health Science, Anhui Science and Technology University, Fengyang, Anhui, 233100, China*

ARTICLE INFO

ABSTRACT

Silver nanoparticles (AgNPs) synthesized from plant extracts have recently emerged as a rapidly growing field with numerous applications in pharmaceutical and clinical contexts. The purpose of this research is to come up with a novel method for the biosynthesis of silver nanoparticles that use *Eucommia ulmoides* leaf extract as a reducing agent. The synthesis of AgNPs was confirmed using UV-vis spectroscopy, and the properties of AgNPs were characterized using Transmission Electron Microscope, Fourier Infrared Spectrometer, X-ray diffraction, Thermogravimetric Analysis, and Zeta potential. The results showed that the AgNPs exhibited a characteristic absorption peak at 430 nm, their diameter ranged from 4 nm to 52 nm, and C, O, and Cl elements, which might represent flavonoids and phenolic components absorbed on the surface of AgNPs. The zeta potential of AgNPs was found to be −30.5 mV, which indicates repulsion among AgNPs and they have good dispersion stability. AgNPs have been found to suppress the tyrosinase activity both in mushroom tyrosinase and A375 cells, as well as diminish ROS formation in HaCat cells. According to this study, AgNPs is a novel material that can enhance skin health by preventing melanin development.

1. Introduction

AgNPs as a nano-product has recently been broadly applied in the biomedical domain [1]. They can be utilized for antimicrobial [2, 3] and anticancer therapies [4], and other biologic functions have been identified, including the promotion of wound repair [5] and bone healing [6] and as vaccine adjuvants [7] and biosensors [8]. There are many methods for synthesizing AgNPs, such as physical [9], chemical [10], and biological [11, 12] methods. Chemical reduction synthesis of AgNPs involves the use of toxic reducing reagents, such as $NaBH_4$, hydrazine, and ethylene glycol [13]. The physical methods usually involve the application of electrical, light, or thermal energy [13]. The biological methods typically use algae [14], fungi [15], and plant extracts as mediators to synthesize AgNPs. The synthesis of AgNPs from plant extracts has become a popular method in recent years [16], and the AgNPs obtained from *Spruce* bark extract, and *Artemisia quttensis Podlech* aerial

part extracts have been reported to have antimicrobial and antioxidant activity [16, 17]. AgNPs synthesized by extract of *Syzygium cumini* were used to compose biocompatible antimicrobial dressings that can accelerate acute wound healing [18]. Many researches showed that the antimicrobial effect, anti-inflammatory activity, and low biotoxicity of AgNPs in tissues make them have great potential for application in skin care [19, 20].

E. ulmoides is an economically important temperate tree species capable of producing wood and several other valuable raw biomaterials, including rubber and the traditional Chinese medicine Duzhong. *E. ulmoides* can tolerate extreme cold and requires fewer soil conditions, it grows in many Chinese provinces, such as Hubei, Henan, and Shanxi. As a result of its widespread planting, it is easier to obtain than many other valuable Chinese herbs due to its extensive planting. *E. ulmoides* has a high medicinal value, and it is commonly employed in Chinese medicine formulations [21], and the mechanism of treatment of various

diseases has been explored [22]. The therapeutic effects of *E. ulmoides* on hypertension, hyperglycemia, diabetes, and Parkinson's disease are remarkable [23]. It has been confirmed to contain a variety of reductive bioactive ingredients such as ulmoidol [24], asperuloside acid, and chlorogenic acid [25]. As a result, we think that using *E. ulmoides* leaf extract to reduce AgNPs is a viable method, and we believe that the AgNPs synthesized by *E. ulmoides* leaf extract will play a great role in specific biological effects.

Therefore, this paper explored the other biological effects of AgNPs synthesized by *E. ulmoides* leaf extract, including the abilities of antioxidant, and anti-tyrosinase activity. We analyzed the influence of AgNPs' concentration on cell viability and explored the biological effect of AgNPs with non-toxic concentrations. The results can provide several references for biological cosmetic industries and consumers.

2. Materials and methods

E. ulmoides leaf extract was purchased from Snuote Biotechnology Co. Ltd. (Shanxi, China). Silver nitrate ($AgNO_3$), disodium hydrogen phosphate (Na_2HPO_4), citric acid monohydrate, L-dopa, and kojic acid were purchased from Aladdin (Shanghai, China). ABTS (2,20 -azino-bis-3- ethylbenzothiazoline-6-sulphonic acid), DPPH (2,2-diphenyl-1-picrylhydrazyl), TPTZ (2,4,6-tri-2-pyridinyl-1,3,5-triazine) and mushroom tyrosinase was obtained from Sigma (Shanghai, China). 5-(and-6)-carboxy-2',7'-dichlorofluorescein diacetate (DCF-DA) and the Heme Oxygenase-1(HO-1) antibodies were purchased from Thermo Fisher Scientific (Shanghai, China). Quinone Oxidoreductase 1 (NQO1) antibodies were purchased from HuaBio (Hangzhou, China). The Human Keratinocytes Cells (HaCat) and Human Malignant Melanoma cells (A375) were purchased from National Collection of Authenticated Cell Cultures (Shanghai, China). Dulbecco's modified eagle medium (DMEM) was purchased from Basal Media (Shanghai, China) for culturing HaCat cells. Fetal bovine serum was obtained from Shenzhen Enduring Biotech Ltd., and the cell counting kit-8 (CCK8) was obtained from Meilunbio (Dalian, China).

2.1. Synthesis of AgNPs

The aqueous solution of *E. ulmoides* leaf extract was prepared by dissolving 0.1 g extract into 10 mL ddH_2O, and then diluted to different concentrations. AgNPs were synthesized by adding $AgNO_3$ solution to an aqueous solution of *E. ulmoides* leaf extract, and the system of extract and $AgNO_3$ was reacted for 24 h in dark at 37 °C. Fifty microliters of $AgNO_3$ (2 M) were added to 10 mL plant extracts at mass fractions of 1%, 0.5%, and 0.1%; the final concentration of $AgNO_3$ was 10 mM. The AgNPs were purified by centrifugation and washed for subsequent experiments. The surface plasmon resonance that exists for metal can be monitored using UV-vis spectrometry [26], so we detected the AgNPs using UV-vis spectrometry in the range of 186 nm to 730 nm. AgNPs were digested by concentrated nitric acid (HNO_3) and then their concentration was determined by ICP-MS (Thermo Fisher Scientific, iCAP RQ). 50 microliters of AgNPs solution were added into 5 mL of concentrated nitric acid in a tube overnight in the dark to nitrolysis, the solution after nitrification was poured into a conical flask, and the tube for nitrification was rinsed with ddH_2O for three times, the wash water was also poured into the conical flask, concentrated nitric acid was heated and evaporated to dryness, and 5 mL of ddH_2O was used to wash the conical flask, the washing liquid was filtered with a polytetrafluoroethylene filter membrane, the filtrate was stored in the dark, and the concentration of Ag in the filtrate was quantified using ICP-MS, using the silver nitrate standard sample as the standard.

2.2. Characterization of AgNPs

2.2.1. FTIR analysis

The AgNPs were synthesized using 1% *E. ulmoides* leaf extract and 10 mM $AgNO_3$ and collected by centrifugation at 10000 rpm for 10 min, and dried for two days using a Freeze drier (Bench Top Pro, Virtis, USA). FTIR spectrometry (VERTEX 80, Germany) was used to ascertain the various functional groups present in the formulated AgNPs in the range of 4000-400 cm^{-1} [27].

2.2.2. TEM and EDS analysis

The AgNPs were synthesized and collected like FTIR. Then the AgNPs were washed three times by adding ddH_2O and centrifuging at 5000 rpm for 20 min and diluted by ddH_2O, transmission electron microscope (FEI Tecnai G2 F20, USA) was used to examine the shape and size of AgNPs. Images were obtained by dispersing the AgNPs onto a copper mesh. Energy-dispersive X-ray was used to analyze the elements of AgNPs.

2.2.3. XRD analysis

The AgNPs were collected like FTIR and dried at 70 °C for 12 h, XRD (Smartlab, Rigaku) was used to examine the crystal structure of AgNPs.

2.2.4. TG analysis

The preparation of AgNPs was like FTIR, and the drying process was the same as the FTIR. Thermal Gravimetric Analyzer (SDT Q600 V20.9 Build 20) was used to analyze the thermal stability of AgNPs, which was carried out under a nitrogen atmosphere with a heating rate of 10 °C/min up to 810 °C. 12.3700 mg was placed into the experimental pan for measurement of weight loss.

2.2.5. DLS analysis

AgNPs were prepared like TEM analysis. Hydrodynamic diameter distribution and zeta potential of AgNPs were measured by Dynamic Light Scattering (Microtrac Nanotrac Wave II).

2.3. Studies in vitro

2.3.1. Free radical scavenging activity by DPPH

The free radical scavenging activity of AgNPs was determined using 2,2-diphenyl-1-picrylhydrazyl (DPPH) [28]. The DPPH working solution was prepared by dissolving 0.009 g DPPH into 90 mL absolute ethyl alcohol. One hundred microliters AgNPs (the sample) or ddH_2O (the blank) were added to 900 μL alcoholic solution of DPPH radical. The solution was mixed evenly and allowed to react at room temperature in the dark. After 30 minutes, the absorbance was measured at 517 nm. Trolox was used as a positive control. The percentage of DPPH radical scavenging was calculated using the equation (1):

$$\text{Scavenging ability} = \left(1 - \frac{A_{sample}}{A_{blank}}\right) \times 100\% \tag{1}$$

2.3.2. ABTS+ scavenging activity assay

ABTS (7 mM) and potassium persulfate (40 mM) were used to prepare the stock ABTS·+ solution (7 mM) [29]. The stock ABTS+ solution was diluted with distilled water to gain the ABTS·+ working solution with an absorbance of 0.75 at 734 nm. Fifty microliters of AgNPs (the sample) or ddH_2O (the blank) were incubated with 200 μL ABTS·+ working solution at room temperature for 6 min, and the absorbance at 734 nm was recorded. Trolox was used as a positive control. The scavenging activity of ABTS·+ was also calculated using the formula (1).

2.3.3. Ferric Reducing Antioxidant Power (FRAP) reducing power assay

Freshly FRAP was obtained following the method reported by Sun et al. [30], which contained acetate buffer (300 mM, pH 3.6), TPTZ solution (10 mM), and ferric chloride solution (20 mM) with the volume proportion at 10:1:1. Fifty microliters AgNPs (the sample) of different concentrations or 50 μL ddH_2O (the blank) and the FRAP reagent (200 μL) were mixed and incubated at room temperature for 30 min. The absorbance of the samples and the blank were recorded at 593 nm

Table 1. The reaction system of mushroom tyrosinase and AgNPs.

	T_{sample}	T_{blank}	C_{sample}	C_{blank}
AgNPs solution (μL)	100	100	——	——
buffer (μL)	——	50	100	150
tyrosinase (μL)	50	——	50	——
L-DOPA (μL)	200	200	200	200

[31]. Trolox was used as the positive control, and the reducing power was represented as the increase in A593, calculated using the formula (2):

$$\text{Reducing power} = \left(A_{sample} - A_{blank} \right) \times 100\% \qquad (2)$$

2.3.4. Anti-tyrosinase activity of mushroom TYR

The *in vitro* inhibition of tyrosinase activity was measured using mushroom tyrosinase (100 U/mL) as previously reported with minor modifications [32]. Fifty microliters of 100 U/mL mushroom tyrosinase solution were mixed with 100 μL AgNPs of different concentrations in a 1.5 mL centrifuge and incubated at 37 °C for 15 min. Two hundred microliters of L-3,4-dihydroxyphenylalanine (L-DOPA, 1 mM) were added, and the solution was incubated at 37 °C in a water bath for 30 min, the reaction system is as Table 1. A microplate reader was used to read the absorbance of dopachrome formation at 475 nm. The result was calculated using the formula (3). T_{sample}: mixtures of AgNPs, tyrosinase and L-DOPA, T_{blank}: mixtures of AgNPs and L-DOPA, C_{sample}: mixtures of tyrosinase and L-DOPA, C_{blank}: only L-DOPA. Disodium hydrogen phosphate-citric acid buffer (pH 6.8) was used to quantify the solution to the same volume.

$$\text{Anti-tyrosinase activity} = \left(1 - \frac{T_{sample} - T_{blank}}{C_{sample} - C_{blank}} \right) \times 100\% \qquad (3)$$

2.4. Studies on cells

2.4.1. Cell culture

A375 and HaCat cells were cultured in Dulbecco's modified eagle medium (DMEM) containing 10% heat-inactivated fetal bovine serum and 1% O-2-deoxy-2-methylamino-α-L-glucopyranosyl-(1→2)-O-5-deoxy-3-C-formyl-α-L-lyxofuranosyl-(1→4)-N1, N3-diamidino-D-streptamine (streptomycin) and 4-Thia-1-azabicyclo [3.2.0] heptane-2-carboxylic acid, 3,3-dimethyl-7-oxo-6-[(2-phenylacetyl) amino]-, (2S, 5R,6R)- (penicillin). The cells were cultured in a 37 °C incubator with 5% CO_2.

2.4.2. Cell viability assay with CCK8

The viability of HaCat cells was tested by cell viability assay using cell counting kit-8 (CCK8), HaCat cells were grown (1×10^4 cells / well) in a 96-well plate for 24 h, and the old medium was substituted with a fresh medium containing serially diluted AgNPs (with concentrations of AgNPs 0, 5, 15, 25, 30, 35, 40, 45 μg/L) and the cells were further incubated for 24 h. After removing the culture medium after 24 h, CCK8 (at the proportion to medium of 1:10) solution was added and the cells were again incubated for 2 h at 37 °C, absorbance was measured using a microplate reader at a wavelength of 450 nm (DNM-9602, Perlong, China).

2.5. Tyrosinase activity in A375 cells

The tyrosinase activity in cells was measured as the reported method [26], the A375 cells were cultured for 24 h before being treated with AgNPs. PBS was used to wash the cells, and 100 μL 10% tween-100 was added to the culture dish, the culture dishes were frozen at −80 °C for 30 minutes and melted at 4 °C, then the cell lysates were centrifuged at 12000 rpm for 15 minutes at 4 °C to clarify. The protein concentrations were determined by the Bradford method and then were adjusted to the same concentration using disodium hydrogen phosphate citrate buffer (pH 6.8). The reaction mixture consisting of 90 μL cell lysates (the sample) or disodium hydrogen phosphate citrate buffer (the control) and 100 μL of 4 mM L-DOPA was added to a 1.5 mL centrifuge tube. And then the mixture of cell lysates and L-Dopa was incubated at 37 °C for 3 h, UV-vis spectrophotometer was used to measure the absorbance at 475 nm. The tyrosinase activity was calculated by the following formula (4):

$$\text{Tyrosinase activity} = \left(\frac{\text{OD}_{475} \text{ of sample}}{\text{OD}_{475} \text{ of control}} \right) \times 100\% \qquad (4)$$

2.5.1. Intracellular ROS detection

5-(and-6)-carboxy-2',7'-dichlorofluorescein diacetate (DCF-DA), the molecular probes sensitive to oxidation, were used to detect the formation of intracellular ROS [33]. For exploring the effect of AgNPs on the ROS level in HaCat cells, the HaCat cells were cultured for 24 h and incubated in wells with different concentrations of AgNPs (0, 5, 15, 25 μg/L) for 24 h, The cells were incubated with 2.5 μM DCF-DA at 37 °C for 20 min in the dark after washing with PBS. The probe can penetrate into the intracellular matrix of cells and is oxidized by ROS to fluoresce. The cells were washed with PBS three times to remove the excess dye, and flow cytometry (BD FACS Aria™, BD Biosciences, China) was used to detect the fluorescence intensity with 488 - nm excitation and 530 - nm emission wavelength. For exploring the effect of AgNPs on the resistance of HaCat against the oxidative stress stimulated by H_2O_2, the cells were incubating with different concentrations of AgNPs (0, 5, 15, 25 μg/L) for 24 h, and washed the cells with PBS, then H_2O_2 (800 μM) was used to stimulate the cells for 2 h. Follow-up experiments are as described above.

2.5.2. Western blot analysis

HaCat cells were cultured for 24 h and incubated with AgNPs for 24 h, and the expressions of the antioxidant protein of HO-1, and NQO1 were analyzed. Cells were lysed with RIPA lysis buffer containing 1% proteinase inhibitor to extract the total protein which was quantified by the Bradford method. Sodium dodecyl sulfate-polyacrylamide gel electrophoresis (SDS-PAGE) was used to separate the samples and transferred them to PVDF membranes. The primary antibodies (HO-1, NQO1, and β-actin) were used to incubate with the PVDF membranes at 4 °C overnight. The next day, secondary anti-mouse or anti-rabbit were then incubated for 2 h at room temperature. Proteins were visualized with the super chemiluminescence substrate ECL (Biosharp, Anhui, China) and imaged using Imager (FluorChem E, Cell Biosciences, AUS), Quantification of band intensity was performed using the Image J Software (NIH, Bethesda, MD, USA).

The procedures of the Bradford method to quantify extracted proteins. First, prepare the working solution in the desired volume (A : B : C = 25 : 24 : 1); Second, add 145 μL of working solution and 5 μL of extracted protein lysate to 96 wells Plate, mix well, incubate at 60 °C for 20 min; Last, use a microplate reader to measure the absorbance at 562 nm; calculate the protein concentration, and use PBS to adjust the protein concentration.

2.6. Statistical analysis

The data were compared by using analysis of variance (ANOVA) with GraphPad Prism software 9.2.0. The results are expressed as the mean ± standard deviation, and the differences were considered significant at $P < 0.05$, ns: $p > 0.05$, $^* p < 0.05$, $^{**} p < 0.01$, and $^{***} p < 0.001$, $^{****} p < 0.0001$.

3. Results and discussion

3.1. Synthesis of AgNPs using E. ulmoides

UV-vis spectrophotometer can be used to determine the formation of AgNPs by observing the characteristic peak [34]. Leaves extract of
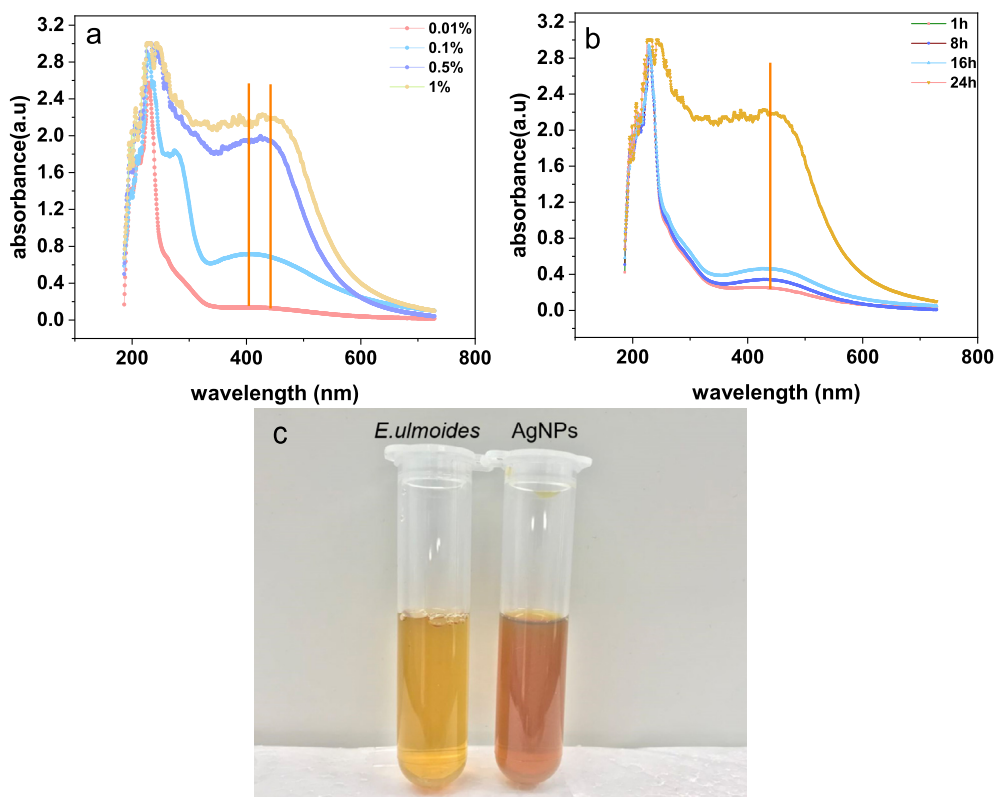
Fig. 1. The adsorption spectrum of AgNPs synthesized by AgNPs (10 mM) and *E. ulmoides* leaf extract with different concentrations (0.01%, 0.1%, 0.5%, 1%) (a), or with different reaction times (1 h, 8 h, 16 h, 24 h) between *E. ulmoides* leaf extract (1%) and AgNO$_3$ (10 mM) (b). The color change of the solution when AgNPs were generated (c).

Acalypha indica was mixed with AgNO$_3$, the solution appears brown because of the surface plasmon vibrations in the AgNPs [35]. The AgNPs synthesized by *E. ulmoides* leaf extract showed absorbance at 430 nm, the peak of AgNPs is broad which is same as the AgNPs synthesized using *Adansonia digitata* L. fruit pulp extract [36]. The intensity of the absorption peak is related to the amount of AgNPs, and the more AgNPs generated, the more intense appeared at the characteristic peak. When 10 mM AgNO$_3$ reacted with 1% extract, the output of AgNPs is more than those AgNPs obtained with 0.01%, 0.1%, and 0.5% extract (Fig. 1a). The 1% extract was reacted with 10 mM AgNO$_3$, and the UV-vis absorption spectrum was measured at 1 h, 8 h, 16 h, and 24 h, respectively; we can learn that the spectrum had the highest peak at 24 h (Fig. 1b). The yield of AgNPs was positively correlated with the concentration of the extract and the reaction time between the extract and AgNO$_3$. The color of the solution changed from pale yellow to yellowish-brown after adding AgNO$_3$ to aqueous solution of *E. ulmoides* leaf extract for 24 hours (Fig. 1c), which indicated the formation of AgNPs. For further analysis, based on the application of Mie's theory, determines the particle sizes from the values of UV-vis absorption spectra [37], because the absorption of light depends on particles' size, shape, aggregation, and so on. The particle size of the AgNPs is larger, the position of the absorption peak will have a red-shift, on the contrary, the absorption peak will have a blue shift [38], and the half-height of the absorption peak is narrower, the distribution of the nanoparticles is more concentrated [39]. Fig. 1a showed that the concentration of extract can influence the particle size of AgNPs, the higher concentration of the extract, the larger the particle size of AgNPs. But the reaction time had no influence on the position of the absorption peak, in another word, it did not affect the particle size of AgNPs (Fig. 1b).
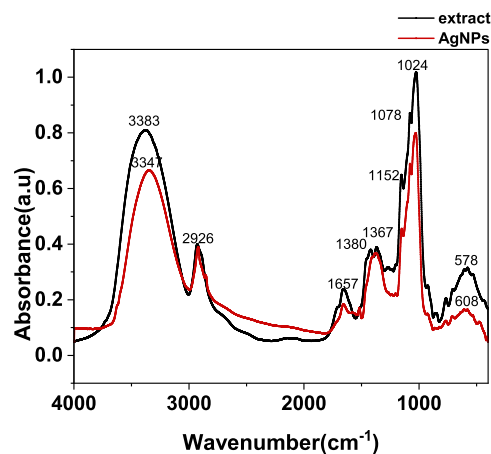

Fig. 2. FTIR spectra of AgNPs and extract of *E. ulmoides* leaf.

3.2. Characterization

3.2.1. FTIR analysis of AgNPs

FTIR analysis was used to know about the function groups participating in the synthesis of AgNPs. As shown in Fig. 2, *E. ulmoides* leaf extract displayed peak near 3383 cm^{-1} could be assigned to N-H stretching vibrations of the secondary amide of protein, the peaks at 2926 and 1657 cm^{-1} that could be due to O-H or C-H and C=C-X stretching vibrations; The absorption peaks at 1380 and 1367 cm^{-1} characteristic stretching of tertiary alcohol (C-OH) and C-X group vibrations, the peak at 1152 and 1078 cm^{-1} correspond to the C-O stretching vibration of alcohol and C-N groups vibrations respectively. The peak at 1024 cm^{-1} could be assigned to the O-H deformation of phenolic OH groups.
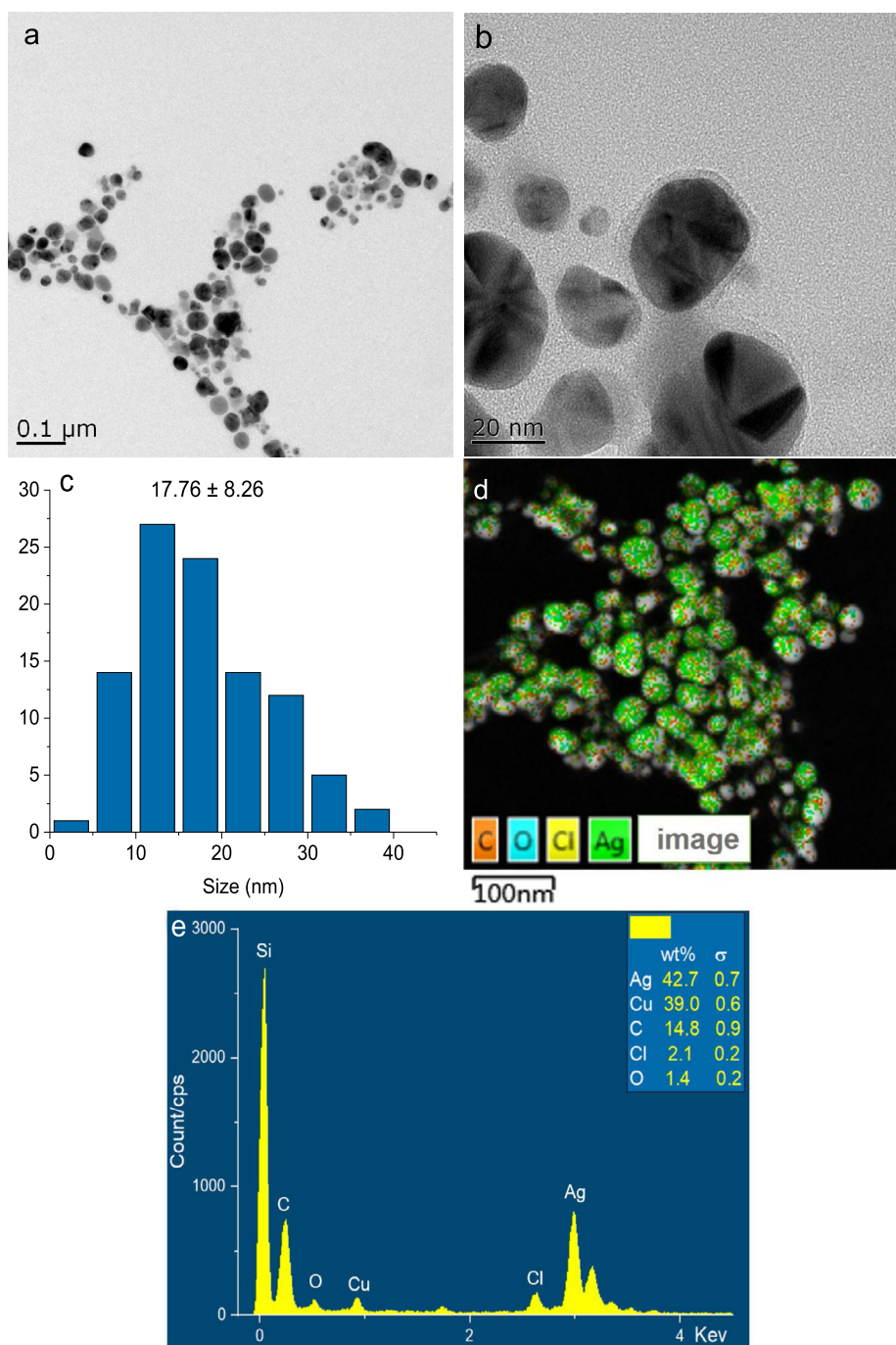
Fig. 3. Transmission electron micrographs of AgNPs (a, b). The histogram of particle size distribution of AgNPs (c). TEM-EDS elemental mapping for Ag, C, Cl, O (d). EDS pattern of synthesized AgNPs (e).

There were several different peaks in the FTIR of AgNPs, the absorption peaks of AgNPs at 3347 and 1380 cm^{-1} which could be deviations from *E. ulmoides* leaf extract. The results clearly showed that the N-H, O-H, and C-X groups may be involved in the synthesis process of AgNPs and adsorbed on the surface of the AgNPs.

3.2.2. TEM analysis of AgNPs

The TEM results indicated that the biosynthesized AgNPs were predominantly irregular sphericity (Fig. 3a). The diameter of AgNPs was analyzed by Image J Software, which was between 4 to 52 nm, we have counted the diameter of 100 particles and got the statistical conclusions: the average diameter is 17.76 nm (Fig. 3c), the standard deviation is 8.26, the minimum is 4.08 nm, and the maximum is 52.7 nm. Fig. 3b

clearly showed that an organic later exists on the surface of AgNPs. We speculated that during the reduction of AgNPs by the *E. ulmoides* extract, some biologically active substances in the *E. ulmoides* extract were attached to the surface of AgNPs.

In order to further verify the surface properties of AgNPs, we analyzed AgNPs using EDS. The EDS mapping is shown in Figs. 3d and 3e, which were used to confirm the presence of AgNPs and elements of C, O, and Cl. The characteristic absorption of metallic silver nanoparticles was at around 3 KeV [40]. The other signals of C, O, and Cl may be due to the biomolecules bound to the surface of the AgNPs (3e). The quantitative analysis showed that Ag has the highest weight of all elements. Combining the result of FTIR, we can draw the conclusion that O-H and C-Cl adsorbed on the surface of AgNPs.
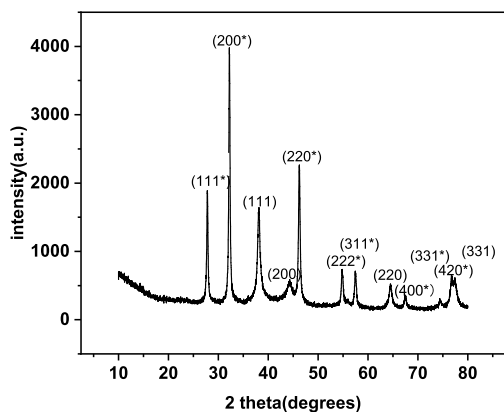
Fig. 4. XRD pattern of AgNPs.

3.2.3. XRD analysis of AgNPs

The X-ray diffraction pattern was used to determine the crystalline properties of AgNPs as shown in Fig. 4. The Bragg reflections with 2θ values of 38.11, 44.30, and 64.44 correspond to the (111), (200), and (220) planes. Using MDI Jade 6 to analyze the data of AgNPs, the data showed that AgNPs were face-centered cubic crystalline phase (PDF2: 87-0597) with a = 4.086 Å. The Bragg reflections with 2θ values of 27.82, 32.24, 46.24, 54.83, 57.48, 67.46, 74.45 and 76.75 attributed to planes (111), (200), (220), (222), (311), (400), (331) and (420) of face-centered cubic phase of AgCl crystal with a = 5.549 Å (PDF2: 85-1355). During the preparation of AgNPs, no chlorine-containing reagent was added, therefore, the AgCl measured by XRD was generated by the reaction between the active substances in the *E. ulmoides* extract and $AgNO_3$. The reaction between $AgNO_3$ and *Derris trifoliata* or *Sonneratia alba* aqueous extracts generated two kinds of nanoparticle (AgNPs and AgCl nanoparticle) [41], Villanuevaibanez et al. [42] using aqueous corn husk extract came to similar conclusions. Based on the following Debye–Scherrer's formula, crystalline size can be estimated [43].

$$D = \frac{K\lambda}{\beta \cos\theta} \tag{5}$$

D: crystalline size, K: constant 0.94, λ: X-Ray wavelength (Cu Ka1, $\lambda = 1.5406$), β: the full width at half the maximum of Braggs peak, convert to radians, $\beta \div 180 \times 3.14$, $\beta = 0.685$, θ: the Bragg angle. From formula (5), the crystalline size is calculated, and the calculated size of AgNPs is 17.0 nm, which is similar to the average size determined by TEM.

3.2.4. DLS analysis

The zeta potential of AgNPs synthesized using *E. ulmoides* extract was −30.5 mV, indicating that negative charge existed on the surface of AgNPs. The value zeta potential was more significant than 30 mV, which confirmed the repulsion among the particles and proved that they are very stable [44].

To further prove the stability of AgNPs, the change of hydrated particle size of AgNPs placed at room temperature for one month was measured, the result was shown in Fig. 5. AgNPs synthesized from extracts of *E. ulmoides* are polydisperse mixtures [45]. The range of hydrated particle size and density distribution of AgNPs did not change significantly within one month, and the AgNPs did not agglomerate, so the AgNPs synthesized from *E. ulmoides* extracts had high stability.

3.2.5. TG analysis

TG was used to analyze further the substances adsorbed on the surface of AgNPs, the results are shown in Fig. 6. The total mass loss was 36.91%, which indicated the presence of bioactive substances on the surface of AgNPs [46, 47].

The temperature reached 150 °C, and the weight loss of AgNPs sample was up to 2.07%, which indicated that the water in AgNPs samples was evaporated. At 150 °C - 290 °C and 290 °C - 620 °C, the weight of
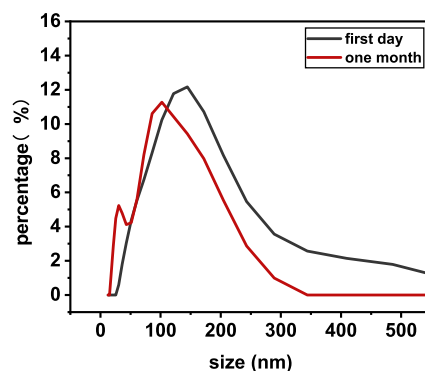

Fig. 5. The change of hydrogen diameter of AgNPs.
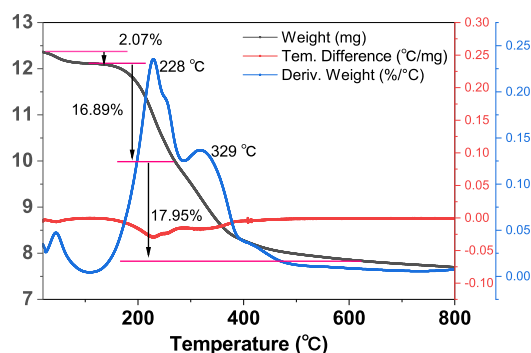
Fig. 6. TGA pattern of AgNPs.

Table 2. Antioxidant capacity of AgNPs.

	DPPH IC$_{50}$ (μg/mL)	ABTS IC$_{50}$ (μg/mL)	FRAP EC$_{50}$ (μg/mL)
AgNPs	50.00 ± 6.84	21.91 ± 5.92	4.52 ± 1.84
Positive control	21.73 ± 0.42	2.54 ± 1.08	2.74 ± 0.10

IC$_{50}$ and EC$_{50}$ values represent the means ± standard deviation of three parallel.

AgNPs decreased by 16.89% and 17.95%, respectively, and the weight loss with temperature peaked at 228 °C and 329 °C, which indicated the degradation of phenolics (the boiling point at 230 °C) and flavonoids, respectively (the boiling point at 367 °C).

3.3. Studies in vitro

3.3.1. Antioxidant activity in vitro

The antioxidant activity of AgNPs was evaluated using three methods. DPPH and ABTS assays were used to evaluate the radical scavenging activity, and the ferric-ion-reducing capacity was detected using FRAP. The IC50 value was defined as an effective concentration for scavenging 50% radical, EC50 was defined as an effective mixture concentration that produces 0.500 absorbance units [30], both the value of IC50 and EC50 was determined from calibration curves, obtained from different concentrations of AgNPs. Table 2 shows the results for the scavenging ability of nano-silver for three kinds of oxidation free radicals. AgNPs showed high DPPH and ABTS scavenging capacities and IC50 values of 50 μg/mL and 21.91 μg/mL, respectively. AgNPs presented reducing power and an EC50 value of 4.52 μg/mL. In this study, the AgNPs synthesized by *E. ulmoides* leaf extract showed potential free-radical scavenging activity, which was achieved by participating in the progress of electron transfer.

The antioxidant capacity of AgNPs obtained by the three methods was compared by the same positive control Trolox as the standard to compare the reduction capacity of AgNPs to DPPH, ABTS, and FRAP, that is, the Trolox equivalent value of the antioxidant capacity of Ag-
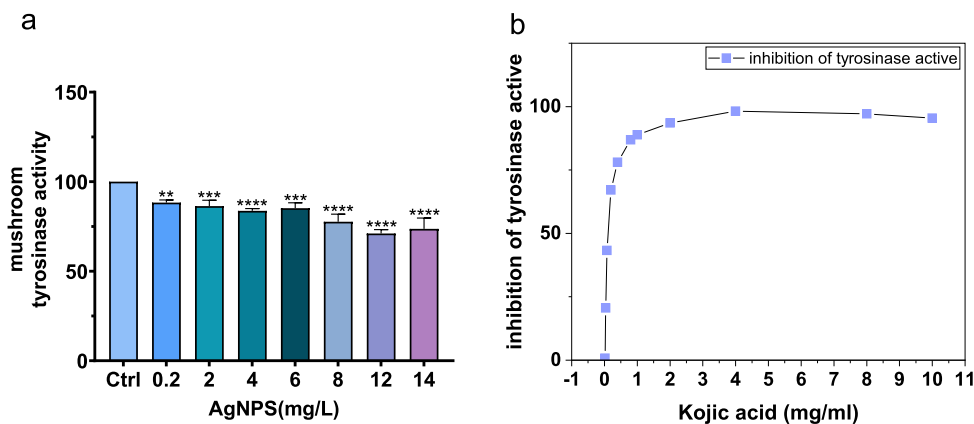
a

b

Fig. 7. Effect of AgNPs on mushroom tyrosinase activity (a). Standard curve of kojic acid inhibiting tyrosinase activity (b).
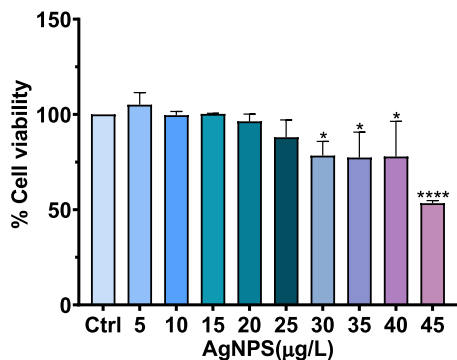

Fig. 8. Effect of AgNPs on HaCat cell viability.
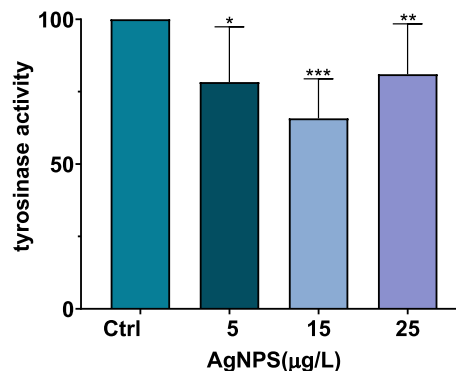

Fig. 9. AgNPs inhibit tyrosinase activity in A375 cells.

NPs. The Trolox equivalent value is defined as the amount of Trolox per 1 molecule of AgNPs.

The results showed that the order of the antioxidant capacity of AgNPs to the three reagents was: FRAP > DPPH > ABTS.

3.3.2. Mushroom tyrosinase activity

As shown in Fig. 7, AgNPs showed obvious inhibition against mushroom tyrosinase activity. In the present study, when the concentration is 0.2 ppm, it already has an inhibitory effect on the enzyme, the most inhibition effect was found to be $28.97 \pm 2.21\%$ when the concentration of AgNPs is 12 mg/L, which is similar to the concentration of kojic acid at 51.61 mg/L. In general, the kojic acid equivalents (KAE/g) stand for the inhibitory ability of per gram AgNPs which equals the corresponding amount of substance (mmol) of kojic acid. In the experiment of this paper, the value of kojic acid equivalents of AgNPs is 29.30 KAE/g.

3.4. Studies on cells

3.4.1. Cytotoxicity of AgNPs on HaCat cells

The effect of AgNPs on HaCat cells viability is displayed in Fig. 8. The result showed that low concentrations of AgNPs did not affect cell viability significantly. Therefore, 5, 15, and 25 μg/L were used in subsequent experiments.

### 3.4.2. Determination of the anti-tyrosinase activity on A375 cells

The tyrosinase activities in A375 cells treated with different concentration of AgNPs (5, 15, 25 μg/L) were found to be $78.0 \pm 19.0\%$, $58.0 \pm 26.5\%$, $81.0 \pm 17.4\%$, respectively (Fig. 9). There is no significant positive correlation between the concentration of AgNPs and the tyrosinase inhibition.

3.4.3. Detection of the antioxidant capacity of AgNPs

We measured the ROS level in HaCat cells incubated with or without AgNPs for 24 h, and the influence of H_2O_2-induced ROS generation on HaCat cells pretreated with or without AgNPs, using flow cytometry. We can draw the following conclusions from Fig. 10. Firstly, AgNPs can lower the intracellular ROS level, the ROS fluorescent intensity peaks in those HaCat cells incubated with AgNPs moved left compared to those without AgNPs (Fig. 10a). Secondly, we stimulated HaCat cells with H_2O_2, and the level of ROS was obviously larger than in the control group, which can be learned from the fluorescent intensity peaks, which means the ROS level in HaCat cells treated with H_2O_2 is higher than those treated without anything. H_2O_2 was used to stimulate HaCat cells that had been pretreated and those that had not been pretreated with AgNPs (5, 15, 25 μg/L) and the ROS level in HaCat cells pretreated using AgNPs was lower than that in the cells did not pretreat with AgNPs. The ability of HaCat cells pretreated with AgNPs to resist oxidative damage induced by H_2O_2 was enhanced (Fig. 10b). The changes in ROS levels in the cells of our control groups and treatment groups were summarized in the histograms (Figs. 10c and 10d). Fig. 10e shows the reason for the antioxidant activities of AgNPs. The up-regulation of HO-1 plays an important role in antioxidant activity, and AgNPs did not affect the expression of NQO1. So, the decrease of ROS in HaCat cells treated with AgNPs was due to the increase of HO-1 expression instead of the NQO1. Studies have shown that a low dose pretreatment of human epithelial cells with AgNPs induced protection against a toxic dose of AgNPs by upregulating the expression of HO-1 [48]. We can say that the concentration of AgNPs we used does not cause oxidative stress and helps to eliminate ROS in cells.

4. Discussion

In recent years, plant extracts have been widely employed to produce silver nanoparticles because they are ecologically benign and
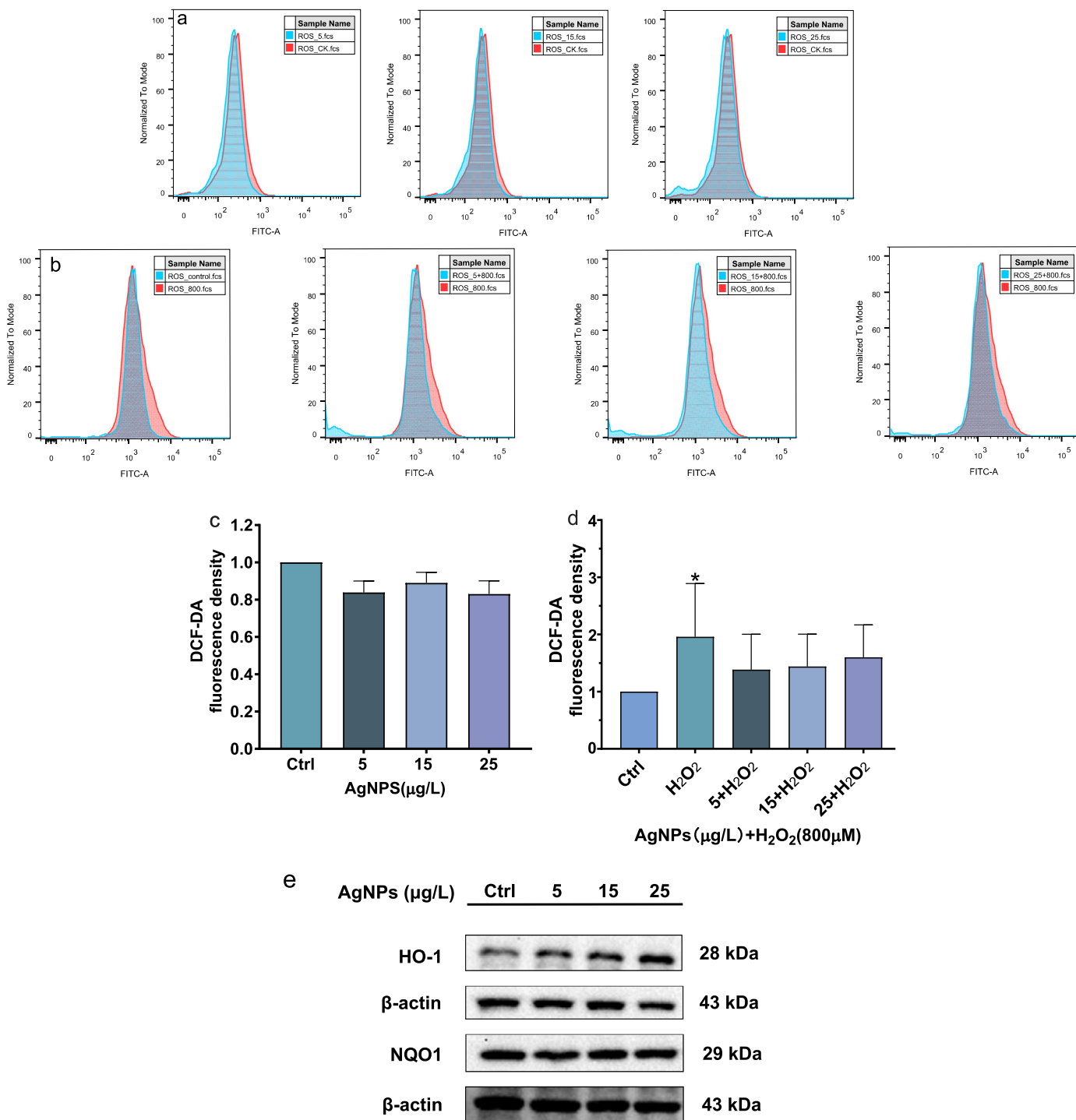
Fig. 10. ROS generation was measured by flow cytometry in HaCat cells. The ROS levels in HaCat cells treated with AgNPs (a). The ROS levels in HaCat cells pretreated with or without AgNPs for 24 h were treated with H_2O_2 (b). Histograms of ROS level changes in HaCat cells (c, d). The protein expression level of HO-1 and NQO1 of HaCat cells that were exposed to 5, 15, 25 μg/L AgNPs for 24 h (e).

biologically less hazardous [49, 50]. Many bioactive compounds in *E. ulmoides* have been identified, including asperuloside, asperulosidic acid, scandoside 10-O-acetate, diacetyl asperulosidic acid, geniposidic acid, aucubin, isoquercetin, quercetin 3-O-sambubioside, rutin, astragalin, kaempherol 3-O-rutinoside, and chlorogenic acid [22]. Using *E. ulmoides* extract to reduce AgNPs has also caught scholars' interest [51, 52], but they only researched the antimicrobial effect, and other biological activities are rarely discussed. So, in this paper, we synthesized AgNPs using *E. ulmoides* leaf extract as a reducing and capping

agent, and characterized the AgNPs using UV-vis spectroscopy, TEM, EDS, FTIR, XRD, DLS and TGA analysis. AgNPs exhibit characteristic absorption peaks on the UV-vis spectrum due to the surface plasmon resonance, and our results confirmed that the UV-vis spectrum of AgNPs displayed absorbance at 430 nm. The biological function of nanoparticles is closely related to particle size, as the size of AgNPs affects the endocytosis in cells [53]. TEM showed the morphology of our AgNPs was irregular sphericity. The average size of the AgNPs synthesized using *E. ulmoides* leaf extract was 17.76 nm, which was comparable to the

AgNPs generated with *Avicennia marina* [11], *Ocimum basilicum*, and *Ocimun sanctum* [54]. XRD yielded a similar conclusion which showed that the diameter of AgNPs is 17 nm. FTIR and EDS mapping analysis were used to identify that -OH and -CCl were the possible functional groups on the surface of AgNPs, and the -OH and -CCl may have contributed to the process of reducing the Ag^+ to AgNPs. Comparing with other research [52] which studied the synthesis of AgNPs using *E. ulmoides* extract (pH 8.0) in the water bath of 60 °C for 40 min, we can draw the conclusion that the conditions on the reaction system between *E. ulmoides* and HNO_3 influenced greatly on AgNPs' physical properties, such as the size and morphology, but the function groups absorbed on the surface of AgNPs did not be effect by reaction conditions, all of our results and others showed that elements of C and O exist on the surface of AgNPs. TG result showed that flavonoids and phenolics was absorbed on the surface of AgNPs based on the weight loss and peak of weight change with temperature. FTIR, EDS, and TG got consistent results which mean bioactive substances exist on the surface of AgNPs.

Tyrosinase is the rate-limiting enzyme in melanin synthesis, that is, inhibiting tyrosinase activity can limit the formation of melanin and then achieve a whitening effect [55], tyrosinase catalyzes tyrosine oxidation to dopaquinone, which is further oxidized to form melanin [56]. It has been reported that AgNPs can inhibit the activity of mushroom tyrosinase [57, 58]. AgNPs can play a great role in inhibiting apoptosis and preventing the formation of wrinkles [59]. But the major literature only performed experiments using chemical reagents, and the inhibition of tyrosinase activity with the influence of AgNPs has always been ignored from a cellular perspective.

AgNPs synthesized using *E. ulmoides* leaf extract were shown to inhibit tyrosinase activity, based on the value of kojic acid equivalents (KAE/g), AgNPs synthesized using *E. ulmoides* leaf extract showed the ability of inhibiting tyrosinase activity, and behaved better than that of AgNPs synthesized by the other plant extracts (*Sideritis brevidens*, *S. lycia*, and *Bidens Frondosa*) [57, 60], Specifically, the value of kojic acid equivalents of Sb-AgNPs, Sl-AgNPs, Bf-AgNPs and our AgNPs is 5.46, 0, 1.11 and 29.30 respectively. To explain the phenomenon, this paper believed the reasons may come from the physicochemical characteristic. The diameter of AgNPs [60] in ranges from 22 to 26 nm with -OH, -C=C-, and -CH; the diameter of AgNPs [61] in ranges from 40 to 50 nm; AgNPs' diameter ranges from 20 to 70 nm with -OH, -NH, and COO- [57], while the average diameter of our AgNPs is 17 nm with -OH, -CCl. It is prima facie evidence in the existing literature that the hydroxyl groups (-OH) of phenolic compounds or flavonoids in the extract can chelate with the copper ions (Cu^{2+}) in mushroom tyrosinase enzyme to limit the activity of tyrosinase [62]. AgNPs have also been shown to interact with copper ion transporters, resulting in chelation of Cu^{2+}, affecting the Cu^{2+} homeostasis of tyrosinase, inhibiting tyrosinase activity [63]. Furthermore, AgNPs have been shown to interact with thiol groups in proteins, resulting in denature of proteins [64]. AgNPs have been found to have significantly higher tyrosinase inhibitory activity compared to plant extracts [57]. We speculated the C-Cl and O-H functional groups on the surface of AgNPs synthesized by the extract have a synergistic effect on the inhibition of mushroom tyrosinase activity by AgNPs. Accordingly, we believe the size and functional group of AgNPs may play an important role in inhibiting tyrosinase activity. Besides, the results also demonstrated that AgNPs hinder the tyrosinase activity of A375 cells, which has not been reported hitherto. *Anthocyanin* can inhibit melanogenesis [26], our AgNPs have an advantage in concentration, specifically, the *Anthocyanin* at the concentration of 5 mg/ml has the same inhibition ability as our AgNPs at 5 μg/L.

Finally, we explored the effect of the concentration of AgNPs on cell viability. When the concentration of AgNPs was lower than 25 μg/L, the cell viability was not affected significantly. Most of the previous results indicated that AgNPs resulted in DNA damage, protein denaturation, and mitochondrial dysfunction through ROS generation, which can inhibit cell proliferation, and induce apoptosis and autophagy, so, AgNPs usually were used in cancer therapies [13]. We found that ROS gener-

ation decreased significantly in HaCat cells treated with AgNPs at less than 25 μg/L. The *in vitro* antioxidant capacity of AgNPs also was confirmed using DPPH, ABTS, and FRAP. The *in vitro* antioxidant capacities of AgNPs have been reported [65, 66], and the AgNPs prepared with natural compounds exhibited antioxidant and anti-inflammatory activities in cells [67]. Additionally, a study has shown that green AgNPs had no significant changes in cell viability, ROS production, or apoptotic changes in HDFa cells at 240 ppm, but AgNPs exhibited an excellent cytotoxic effect on tumor cells [68]. Amooaghaie et al. proved that cytotoxicity of the green synthesized AgNPs (using leaf extract of *Nigella sativa*) was significantly less than wet-chemistry synthesized ones (using sodium borohydride and sodium citrate) [69]. AgNPs synthesized using cell-free filtrates from the fungus displayed less toxicity than chemical AgNPs in the model organism *Caenorhabditis elegans*, which is due to the proteins capping on the surface of bio-AgNPs [70]. Sur et al. [71] investigated the cytotoxicity of naked AgNPs and AgNPs modified with glucose, lactose, and oligonucleotides on A549 cells, and the result showed that only naked AgNPs influence the viability of the A549 cells. The coating substances of AgNPs will affect their antioxidant capacity. EG-AgNPs (capping with Ethylene glycol) determined protective antioxidant effects in a dose-dependent, however, PVP-EG-AgNPs (capping with Polyvinylpyrrolidone) showed a different trend compared to EG-AgNPs [72]. So, we thought those flavonoid and phenolic substances absorbed on the surface of AgNPs synthesized using *E. ulmoides* extracts are the major reason for the excellent antioxidant ability and the less cytotoxicity than chemical and physical AgNPs. Studies have shown that surface charge affects the biological toxicity of AgNPs [73], the binding ability of negatively charged AgNPs is weak to biomolecules such as proteins and nucleic acids, therefore, negatively charged AgNPs are less cytotoxic than positively charged AgNPs [74], the zeta potential of our AgNPs is −30.5 mV, which provided safety proof for the application of AgNPs synthesized by *E. ulmoides*. Therefore, AgNPs may be used in cosmetics in the future. Low doses of AgNPs did not affect cell viability and had a certain effect on whitening.

5. Conclusion

In this study, we synthesized the AgNPs using *E. ulmoides* leaf extract, and analyzed their physicochemical characters, then explored the biological and chemical effects of our AgNPs further. The AgNPs synthesized by *E. ulmoides* leaf extract showed strong antioxidant properties and anti-TYR activity in both *in vitro* and cell experiments under the condition of not affecting the cell viability. So, our study shows that AgNPs can be used as a whitening product in the cosmetics field.

Declarations

Author contribution statement

Jinfeng Xi: Conceived and designed the experiments; Performed the experiments; Analyzed and interpreted the data; Wrote the paper.

Wenjie Kan, Yan Zhu: Analyzed and interpreted the data.

Shengwei Huang, Lifang Wu, Jun Wang: Conceived and designed the experiments; Contributed reagents, materials, analysis tools or data.

Funding statement

This work was supported by the Biological Resources Programme, Chinese Academy of Sciences (KFJ-BRP-007-014), the President Foundation of Hefei Institute of Physical Science of Chinese Academy of Sciences (YZJJZX202013), the Foundation for Talented Scholars from the city of Sanmenxia and the Elite Program from the city of Xuchang.

Data availability statement

Data will be made available on request.

Declaration of interests statement

The authors declare no conflict of interest.

Additional information

No additional information is available for this paper.

References

[1] X. Chen, H.J. Schluesener, Nanosilver: a nanoproduct in medical application, Toxicol. Lett. 176 (1) (2008) 1–12.

[2] S. Prabhu, E.K. Poulose, Silver nanoparticles: mechanism of antimicrobial action, synthesis, medical applications, and toxicity effects, Int. Nano Lett. 2 (1) (2012) 1–10.

[3] J. Zhang, G. Duan, Y. Fu, J. Zhao, Preparation of the egg membrane bandage contained the antibacterial Ag nanoparticles, Mater. Charact. 100 (2015) 207–211.

[4] J. Lin, Z. Huang, H. Wu, W. Zhou, P. Jin, P. Wei, Y. Zhang, F. Zheng, J. Zhang, J. Xu, et al., Inhibition of autophagy enhances the anticancer activity of silver nanoparticles, Autophagy 10 (11) (2014) 2006–2020.

[5] S. Chowdhury, M. De, R. Guha, S. Batabyal, I. Samanta, S.K. Hazra, T.K. Ghosh, A. Konar, S. Hazra, Influence of silver nanoparticles on post-surgical wound healing following topical application, Eur. J. Nanomed. 6 (4) (2014) 237–247.

[6] E. Marsich, F. Bellomo, G. Turco, A. Travan, I. Donati, S. Paoletti, Nano-composite scaffolds for bone tissue engineering containing silver nanoparticles: preparation, characterization and biological properties, J. Mater. Sci., Mater. Med. 24 (7) (2013) 1799–1807.

[7] P. Orłowski, A. Kowalczyk, E. Tomaszewska, K. Ranoszek-Soliwoda, A. Węgrzyn, J. Grzesiak, G. Celichowski, J. Grobelny, K. Eriksson, M. Krzyzowska, Antiviral activity of tannic acid modified silver nanoparticles: potential to activate immune response in herpes genitalis, Viruses 10 (10) (2018) 524.

[8] A. Loiseau, V. Asila, G. Boitel-Aullen, M. Lam, M. Salmain, S. Boujday, Silver-based plasmonic nanoparticles for and their use in biosensing, Biosensors 9 (2) (2019) 78.

[9] V. Amendola, M. Meneghetti, Laser ablation synthesis in solution and size manipulation of noble metal nanoparticles, Phys. Chem. Chem. Phys. 11 (20) (2009) 3805–3821.

[10] X. Jiang, W. Chen, C. Chen, S. Xiong, A. Yu, Role of temperature in the growth of silver nanoparticles through a synergetic reduction approach, Nanoscale Res. Lett. 6 (1) (2011) 32.

[11] V. Abdi, I. Sourinejad, M. Yousefzadi, Z. Ghasemi, Mangrove-mediated synthesis of silver nanoparticles using native *Avicennia marina* plant extract from southern Iran, Chem. Eng. Commun. 205 (8) (2018) 1069–1076.

[12] Y. Zhang, X. Cheng, Y. Zhang, X. Xue, Y. Fu, Biosynthesis of silver nanoparticles at room temperature using aqueous aloe leaf extract and antibacterial properties, Colloids Surf. A, Physicochem. Eng. Asp. 423 (2013) 63–68.

[13] L. Xu, Y.-Y. Wang, J. Huang, C.-Y. Chen, Z.-X. Wang, H. Xie, Silver nanoparticles: synthesis, medical applications and biosafety, Theranostics 10 (20) (2020) 8996.

[14] D. Chugh, V. Viswamalya, B. Das, Green synthesis of silver nanoparticles with algae and the importance of capping agents in the process, J. Gen. Eng. Biotechnol. 19 (1) (2021) 1–21.

[15] X. Zhao, L. Zhou, M.S. Riaz Rajoka, L. Yan, C. Jiang, D. Shao, J. Zhu, J. Shi, Q. Huang, H. Yang, et al., Fungal silver nanoparticles: synthesis, application and challenges, Crit. Rev. Biotechnol. 38 (6) (2018) 817–835.

[16] C. Tanase, L. Berta, N.A. Coman, I. Roșca, A. Man, F. Toma, A. Mocan, A. Nicolescu, L. Jakab-Farkas, D. Biró, et al., Antibacterial and antioxidant potential of silver nanoparticles biosynthesized using the spruce bark extract, Nanomaterials 9 (11) (2019) 1541.

[17] F. Ghanbar, A. Mirzaie, F. Ashrafi, H. Noorbazargan, M.D. Jalali, S. Salehi, S.A.S. Shandiz, Antioxidant, antibacterial and anticancer properties of phyto-synthesised *Artemisia quttensis Podlech* extract mediated AgNPs, IET Nanobiotechnol. 11 (4) (2017) 485–492.

[18] R. Singla, S. Soni, V. Patial, P.M. Kulurkar, A. Kumari, S. Mahesh, Y.S. Padwad, S.K. Yadav, Cytocompatible anti-microbial dressings of *Syzygium cumini* cellulose nanocrystals decorated with silver nanoparticles accelerate acute and diabetic wound healing, Sci. Rep. 7 (1) (2017) 1–13.

[19] M. Rahimi, E.B. Noruzi, E. Sheykhsaran, B. Ebadi, Z. Kariminezhad, M. Molaparast, M.G. Mehrabani, B. Mehramouz, M. Yousefi, R. Ahmadi, et al., Carbohydrate polymer-based silver nanocomposites: recent progress in the antimicrobial wound dressings, Carbohydr. Polym. 231 (2020) 115696.

[20] S.P. Deshmukh, S. Patil, S. Mullani, S. Delekar, Silver nanoparticles as an effective disinfectant: a review, Mater. Sci. Eng. C 97 (2019) 954–965.

[21] X. He, J. Wang, M. Li, D. Hao, Y. Yang, C. Zhang, R. He, R. Tao, *Eucommia ulmoides* Oliv.: ethnopharmacology, phytochemistry and pharmacology of an important traditional Chinese medicine, J. Ethnopharmacol. 151 (1) (2014) 78–92.

[22] Y. Li, C. Han, J. Wang, W. Xiao, Z. Wang, J. Zhang, Y. Yang, S. Zhang, C. Ai, Investigation into the mechanism of *Eucommia ulmoides* Oliv. based on a systems pharmacology approach, J. Ethnopharmacol. 151 (1) (2014) 452–460.

[23] L. Huang, Q. Lyu, W. Zheng, Q. Yang, G. Cao, Traditional application and modern pharmacological research of *Eucommia ulmoides* Oliv., Chin. Med. 16 (1) (2021) 1–26.

[24] C. Tanaka, T. Nakamura, Y. Nakazawa, T. Nohara, A new triterpenoid from the leaves of *Eucommia ulmoides* OLIV., Chem. Pharm. Bull. 45 (8) (1997) 1379–1380.

[25] C. Takamura, T. Hirata, Y. Yamaguchi, M. Ono, H. Miyashita, T. Ikeda, T. Nohara, Studies on the chemical constituents of green leaves of *Eucommia ulmoides* Oliv., J. Nat. Med. 61 (2) (2007) 220–221.

[26] J.-M. Hwang, H.-C. Kuo, C.-T. Lin, E.-S. Kao, Inhibitory effect of liposome-encapsulated anthocyanin on melanogenesis in human melanocytes, Pharm. Biol. 51 (8) (2013) 941–947.

[27] M.F. Zayed, W.H. Eisa, Y.K. Abdel-Moneam, S.M. El-Kousy, A. Atia, Ziziphus spina-christi based bio-synthesis of Ag nanoparticles, J. Ind. Eng. Chem. 23 (2015) 50–56.

[28] K. Dumri, S. Letsiri, Pro-oxidative activity in some Thai spices, in: III WOCMAP Congress on Medicinal and Aromatic Plants, vol. 6: Traditional Medicine and Nutraceuticals, vol. 680, 2003, pp. 25–29.

[29] R. Re, N. Pellegrini, A. Proteggente, A. Pannala, M. Yang, C. Rice-Evans, Antioxidant activity applying an improved ABTS radical cation decolorization assay, Free Radic. Biol. Med. 26 (9–10) (1999) 1231–1237.

[30] L. Sun, Y. Guo, Y. Zhang, Y. Zhuang, Antioxidant and anti-tyrosinase activities of phenolic extracts from rape bee pollen and inhibitory melanogenesis by cAMP/MITF/TYR pathway in B16 mouse melanoma cells, Front. Pharmacol. 8 (2017) 104.

[31] C. Hou, L. Wu, Z. Wang, E. Saguer, D. Zhang, Purification and identification of antioxidant alcalase-derived peptides from sheep plasma proteins, Antioxidants 8 (12) (2019) 592.

[32] G. Zengin, S. Uysal, R. Ceylan, A. Aktumsek, Phenolic constituent, antioxidative and tyrosinase inhibitory activity of *Ornithogalum narbonense* L. from Turkey: a phytochemical study, Ind. Crop. Prod. 70 (2015) 1–6.

[33] J. Tavakkol-Afshari, A. Brook, S.H. Mousavi, Study of cytotoxic and apoptogenic properties of saffron extract in human cancer cell lines, Food Chem. Toxicol. 46 (11) (2008) 3443–3447.

[34] L. Amarasinghe, P. Wickramarachchi, A. Aberathna, W. Sithara, C. De Silva, Comparative study on larvicidal activity of green synthesized silver nanoparticles and Annona glabra (Annonaceae) aqueous extract to control Aedes aegypti and Aedes albopictus (Diptera: Culicidae), Heliyon 6 (6) (2020) e04322, https://www.sciencedirect.com/science/article/pii/S240584402031166X.

[35] C. Krishnaraj, E. Jagan, S. Rajasekar, P. Selvakumar, P. Kalaichelvan, N. Mohan, Synthesis of silver nanoparticles using *Acalypha indica* leaf extracts and its antibacterial activity against water borne pathogens, Colloids Surf. B, Biointerfaces 76 (1) (2010) 50–56.

[36] C.M.K. Kumar, P. Yugandhar, N. Savithramma, Biological synthesis of silver nanoparticles from Adansonia digitata L. fruit pulp extract, characterization, and its antimicrobial properties, J. Intercult. Ethnopharmacol. 5 (1) (2016) 79.

[37] C. Contado, R. Argazzi, V. Amendola, Sedimentation field flow fractionation and optical absorption spectroscopy for a quantitative size characterization of silver nanoparticles, J. Chromatogr. A 1471 (2016) 178–185.

[38] N. Jafarzadeh, M. Nadafan, R. Malekfar, A. Shakeri-Zadeh, A. Meidanchi, S. Eynali, Structural, optical and dielectric studies of Ag nanoparticles decorated by herceptin, Physica E, Low-Dimens. Syst. Nanostruct. 114 (2019) 113562.

[39] A. Alahmad, A. Feldhoff, N.C. Bigall, P. Rusch, T. Scheper, J.-G. Walter, *Hypericum perforatum L.*-mediated green synthesis of silver nanoparticles exhibiting antioxidant and anticancer activities, Nanomaterials 11 (2) (2021) 487.

[40] A. Aravinthan, M. Govarthanan, K. Selvam, L. Praburaman, T. Selvankumar, R. Balamurugan, S. Kamala-Kannan, J.-H. Kim, Sunroot mediated synthesis and characterization of silver nanoparticles and evaluation of its antibacterial and rat splenocyte cytotoxic effects, Int. J. Nanomed. 10 (2015) 1977.

[41] P. Gawali, B. Jadhav, Synthesis of Ag/AgCl nanoparticles and their action on human serum albumin: a fluorescence study, Process Biochem. 69 (2018) 106–122.

[42] M. Villanueva-Ibáñez, M. Yañez-Cruz, R. Álvarez García, M. Hernández-Pérez, M. Flores-González, Aqueous corn husk extract – mediated green synthesis of AgCl and Ag nanoparticles, Mater. Lett. 152 (2015) 166–169.

[43] B. Cullity, Measurement of Residual Stress, Elements of X-Ray Diffraction, 2nd ed., Addison-Wesley, Massachusetts, 1978, pp. 447–476.

[44] Y.S. Rao, V.S. Kotakadi, T. Prasad, A.V. Reddy, D.S. Gopal, Green synthesis and spectral characterization of silver nanoparticles from *Lakshmi tulasi (Ocimum sanctum)* leaf extract, Spectrochim. Acta, Part A, Mol. Biomol. Spectrosc. 103 (2013) 156–159.

[45] S. Umoren, I. Obot, Z. Gasem, Green synthesis and characterization of silver nanoparticles using red apple *(Malus domestica)* fruit extract at room temperature, J. Mater. Environ. Sci. 5 (3) (2014) 907–914.

[46] T.T.T. Tran, T.T.H. Vu, T.H. Nguyen, Biosynthesis of silver nanoparticles using Tithonia diversifolia leaf extract and their antimicrobial activity, Mater. Lett. 105 (2013) 220–223.

[47] J.F. Priyadarshini, K. Sivakumari, R. Selvaraj, K. Ashok, P. Jayaprakash, S. Rajesh, Green synthesis of silver nanoparticles from propolis, Res. J. Life Sci. Bioinform. Pharm. Chem. Sci. 4 (2018) 23–36.

[48] M.M. Sthijns, W. Thongkam, C. Albrecht, B. Hellack, A. Bast, G.R. Haenen, R.P. Schins, Silver nanoparticles induce hormesis in A549 human epithelial cells, Toxicol. in Vitro 40 (2017) 223–233.

[49] M. Ali, B. Kim, K.D. Belfield, D. Norman, M. Brennan, G.S. Ali, Green synthesis and characterization of silver nanoparticles using *Artemisia absinthium* aqueous extract—a comprehensive study, Mater. Sci. Eng. C 58 (2016) 359–365.

[50] S. Rajeshkumar, L. Bharath, Mechanism of plant-mediated synthesis of silver nanoparticles–a review on biomolecules involved, characterisation and antibacterial activity, Chem.-Biol. Interact. 273 (2017) 219–227.

[51] Y. Yang, T. Zhao, T. Zhang, Synthesis of silver nanoparticles via traditional Chinese medicine and evaluation of their antibacterial activities, RSC Adv. 11 (47) (2021) 29519–29526.

[52] S. Lü, Y. Wu, H. Liu, Silver nanoparticles synthesized using *Eucommia ulmoides* bark and their antibacterial efficacy, Mater. Lett. 196 (2017) 217–220.

[53] M. Wu, H. Guo, L. Liu, Y. Liu, L. Xie, Size-dependent cellular uptake and localization profiles of silver nanoparticles, Int. J. Nanomed. 14 (2019) 4247.

[54] V. Malapermal, I. Botha, S.B.N. Krishna, J.N. Mbatha, Enhancing antidiabetic and antimicrobial performance of *Ocimum basilicum*, and *Ocimum sanctum (L.)* using silver nanoparticles, Saudi J. Biol. Sci. 24 (6) (2017) 1294–1305.

[55] V.J. Hearing, K. Tsukamoto, Enzymatic control of pigmentation in mammals, FASEB J. 5 (14) (1991) 2902–2909.

[56] T.-S. Chang, An updated review of tyrosinase inhibitors, Int. J. Mol. Sci. 10 (6) (2009) 2440–2475.

[57] M.S. Qamar Abbas, A.R. Phull, M. Rafiq, M. Hassan, K.-H. Lee, S.-Y. Seo, Green synthesis of silver nanoparticles using *Bidens frondosa* extract and their tyrosinase activity, Iran. J. Pharm. Res. 16 (2) (2017) 763.

[58] E. Mostafa, M.A. Fayed, R.A. Radwan, R.O. Bakr, *Centaurea pumilio L.* extract and nanoparticles: a candidate for healthy skin, Colloids Surf. B, Biointerfaces 182 (2019) 110350.

[59] R.A. Radwan, Y.A. El-Sherif, M.M. Salama, A novel biochemical study of anti-ageing potential of *Eucalyptus camaldulensis* bark waste standardized extract and silver nanoparticles, Colloids Surf. B, Biointerfaces 191 (2020) 111004.

[60] R. Ceylan, A. Demirbas, I. Ocsoy, A. Aktumsek, Green synthesis of silver nanoparticles using aqueous extracts of three Sideritis species from Turkey and evaluations bioactivity potentials, Sustain. Chem. Pharm. 21 (2021) 100426.

[61] N. Basavegowda, A. Idhayadhulla, Y.R. Lee, Tyrosinase inhibitory activity of silver nanoparticles treated with *Hovenia dulcis* fruit extract: an in vitro study, Mater. Lett. 129 (2014) 28–30.

[62] G. Battaini, E. Monzani, L. Casella, L. Santagostini, R. Pagliarin, Inhibition of the catecholase activity of biomimetic dinuclear copper complexes by kojic acid, J. Biol. Inorg. Chem. 5 (2) (2000) 262–268.

[63] N. Armstrong, M. Ramamoorthy, D. Lyon, K. Jones, A. Duttaroy, Mechanism of silver nanoparticles action on insect pigmentation reveals intervention of copper homeostasis, PLoS ONE 8 (1) (2013) e53186.

[64] H.J. Johnston, G. Hutchison, F.M. Christensen, S. Peters, S. Hankin, V. Stone, A review of the *in vivo* and *in vitro* toxicity of silver and gold particulates: particle attributes and biological mechanisms responsible for the observed toxicity, Crit. Rev. Toxicol. 40 (4) (2010) 328–346.

[65] D.A. Selvan, D. Mahendiran, R.S. Kumar, A.K. Rahiman, Garlic, green tea and turmeric extracts-mediated green synthesis of silver nanoparticles: phytochemical, antioxidant and in vitro cytotoxicity studies, J. Photochem. Photobiol. B, Biol. 180 (2018) 243–252.

[66] S. Palanisamy, P. Rajasekar, G. Vijayaprasath, G. Ravi, R. Manikandan, N.M. Prabhu, A green route to synthesis silver nanoparticles using Sargassum polycystum and its antioxidant and cytotoxic effects: an in vitro analysis, Mater. Lett. 189 (2017) 196–200.

[67] L. David, B. Moldovan, I. Baldea, D. Olteanu, P. Bolfa, S. Clichici, G.A. Filip, Modulatory effects of *Cornus sanguinea L.* mediated green synthesized silver nanoparticles on oxidative stress, COX-2/NOS2 and NFkB/pNFkB expressions in experimental inflammation in Wistar rats, Mater. Sci. Eng. C 110 (2020) 110709.

[68] S. Kummara, M.B. Patil, T. Uriah, Synthesis, characterization, biocompatible and anticancer activity of green and chemically synthesized silver nanoparticles–a comparative study, Biomed. Pharmacother. 84 (2016) 10–21.

[69] R. Amooaghaie, M.R. Saeri, M. Azizi, Synthesis, characterization and biocompatibility of silver nanoparticles synthesized from *Nigella sativa* leaf extract in comparison with chemical silver nanoparticles, Ecotoxicol. Environ. Saf. 120 (2015) 400–408.

[70] F.N. Spagnoletti, F. Kronberg, C. Spedalieri, E. Munarriz, R. Giacometti, Protein corona on biogenic silver nanoparticles provides higher stability and protects cells from toxicity in comparison to chemical nanoparticles, J. Environ. Manag. 297 (2021) 113434.

[71] I. Sur, D. Cam, M. Kahraman, A. Baysal, M. Culha, Interaction of multi-functional silver nanoparticles with living cells, Nanotechnology 21 (17) (2010) 175104.

[72] A.O. Docea, D. Calina, A.M. Buga, O. Zlatian, M. Paoliello, G.D. Mogosanu, C.T. Streba, E.L. Popescu, A.E. Stoica, A.C. Bîrcă, et al., The effect of silver nanoparticles on antioxidant/pro-oxidant balance in a murine model, Int. J. Mol. Sci. 21 (4) (2020) 1233.

[73] A.M. El Badawy, R.G. Silva, B. Morris, K.G. Scheckel, M.T. Suidan, T.M. Tolaymat, Surface charge-dependent toxicity of silver nanoparticles, Environ. Sci. Technol. 45 (1) (2011) 283–287.

[74] A.K. Suresh, D.A. Pelletier, W. Wang, J.L. Morrell-Falvey, B. Gu, M.J. Doktycz, Cytotoxicity induced by engineered silver nanocrystallites is dependent on surface coatings and cell types, Langmuir 28 (5) (2012) 2727–2735.